Biochemistry and Biophysics Reports 36 (2023) 101581

Contents lists available at ScienceDirect

Biochemistry and Biophysics Reports

journal homepage: www.elsevier.com/locate/bbrep

Computational biology of antibody epitope, tunnels and pores analysis of protein glutathione S-transferase P, and quantum mechanics

Uma Maheswari Chandramohan

Department of Physics, VelTech HighTech Dr. Rangarajan Dr. Sakunthala Engineering College, Avadi, Chennai, 600062, Tamilnadu, India

ARTICLE INFO

Keywords:
Molecular geometry
Vibrational assignment
Wave function
Molecular docking
Antibody epitope
Protein tunnels and pores analysis

ABSTRACT

Different tissues of various plants contain allelochemicals such as phenolics, flavonoids, etc., which exhibit antioxidants and protect the plants from harmful infections. The widespread group of plant allelochemicals in the ecosystem is phenolic compounds. They are substances composed of an aromatic hydrocarbon group and a hydroxyl group. The 3-Hydroxyflavone skeleton of flavonol has a phenolic and a hydroxyl substitution. A comparison of experimental and calculated data of FT-IR and Raman was studied for the vibrational assessment of these allelochemicals. PES scan and molecular geometry analysis are done for the conformation of the 3-Hydroxyflavone ligand. 3-Hydroxyflavone is docked with the three proteins of Homo sapiens such as **Prothrombin with 622 amino acids** synthesized in the liver, human neutrophils found within intracellular granules with 467 amino acids, **Glutathione S-transferase P is produced from** exogenous xenobiotics with 210 amino acids. The active site residues by using the **Prothrombin** (1A2C), **Neutrophil collagenase** (1A86), **Glutathione S-transferase P**(18 GS) protein with ligand 3-Hydroxyflavone, fair binding affinity was found for the **Glutathione S-transferase P** (18 GS). The MOLE online server web interface's ability to see and analyze tunnels and pores allows for simple, online interaction with bio-macromolecule investigation. The automatic transmembrane channel calculation on the MOLE web generates the quickest list of ligands for transport analysis and tunnel identification. Pore-forming proteins (PFPs) are recognized as crucial agents in immunity and infection. They target membranes by opening channels through them. ElliPro is thought to be a potentially effective method for identifying antibody epitopes in protein antigens. Molecular dynamics result the general time-dependent structural deviation/degree of similarity among the structures that the trajectory records. The epitope technique sought to examine the effectiveness of its web tool on linear and discontinuous epitopes known from the structures of antibodies of 18 GS with 3-Hydroxyflavone complexes and find effective scores.

1. Introduction

Natural compounds from plants provide recent research opportunities due to their remarkable pharmacological and pharmacoepidemiology properties. The secondary metabolite Polyphenols from plants are involved in defense against aggression by pathogens. Flavonoids from polyphenolic secondary metabolites have a wide spectrum of pharmacological activities such as anticancer, antiviral, antifungal, antibacterial, antioxidant, cardioprotective, immunomodulatory, and anti-inflammatory [1]. Plants are shielded from various biotic and abiotic challenges by flavonoids, which also serve as special UV filters, signaling molecules, allopathic substances, phytoalexins, detoxifying agents, and antimicrobial defensive components [2].

Flavonol is the unsaturated C ring at the C2–C3 position, which is hydroxylated at C3 and oxidized at C4. Flavonol is a group of flavonoids that are mainly accumulated in epidermal cells of plant tissues in response to solar radiation to filter the UV-B light while allowing it to pass the photosynthetically active visible light [3]. 3-Hydroxyflavone is a natural product found in Acacia retinoids, Acacia holosericea, and other organisms. Meta-analyses strongly suggested that long-term consumption of diets rich in plant polyphenols offered some protection against the development of cancers, cardiovascular diseases, diabetes, osteoporosis, and neurodegenerative diseases [4,5].

Recent research on various plant metabolites has demonstrated that flavonoids may play a major role in the brain's enzyme and receptor systems, having a major impact on the central nervous system and preventing diseases like Alzheimer's and Parkinson's [6,7]. They are building blocks of proanthocyanins and the intake of flavonol is found to be associated with a wide range of health benefits which include antioxidant potential and reduced risk of vascular disease [8]. Flavonoids

E-mail address: umas.umas@gmail.com.

https://doi.org/10.1016/j.bbrep.2023.101581
Received 30 September 2023; Received in revised form 4 November 2023; Accepted 7 November 2023
2405-5808/© 2023 Published by Elsevier B.V. This is an open access article under the CC BY-NC-ND license (http://creativecommons.org/licenses/by-nc-nd/4.0/).

Table 1
Optimized parameters of [bond length (Å), bond angle (°)] 3-Hydroxyflavone.

Parameters	Experimental[a]	B3LYP/6-31G (d, p)	Parameters	Experimental[a]	B3LYP/6-31G (d, p)
Bond Length			Bond Angle		
C1–C2	1.363	1.366	C2–C1–O11	119.7	121.8
C1–C12	1.474	1.475	O11–C1–C12	111.1	111.9
C1–O11	1.369	1.373	C1–C2–C3	122.8	121.6
C2–C3	1.457	1.473	C1–C2–O18	120.8	124.0
C2–O18	1.357	1.361	C2–C3–C4	119.8	122.6
C3–O4	1.232	1.227	C2–C3–C5	116	113.9
C3–C5	1.446	1.475	C5–C6–C7	121.2	120.5
C5–C6	1.387	1.406	C7–C8–C9	120.1	120.7
C6–C7	1.366	1.384	C8–C9–C10	118.7	118.7
C7–C8	1.372	1.406	C9–C10–O11	115.4	116.8
C8–C9	1.385	1.387	C13–C12–C17	119.4	118.6
C9–C10	1.392	1.400	C12–C13–C14	121.3	120.4
C10–11O	1.377	1.364	C13–C14–C15	120	120.3
C12–C13	1.394	1.406	C14–C15–C16	118.5	119.6
C12–C17	1.389	1.407	C15–C16–C17	121.3	120.2
C13–C14	1.397	1.391	C2–O18–H28	109	109.2
C14–C15	1.377	1.397	C12–C1–C13	119.4	120
C15–C16	1.400	1.394			
C16–C17	1.364	1.394			
O18–H28	0.96	0.968			

[a] Ref: [30].

are effective antibacterial agents whose bactericidal potential is dictated by their chemical structures and concentrations.

Aglycones and their glycosylated and methylated derivatives are known forms of flavonoids. In the human diet, glycosylated flavonoids are widely distributed [9]. Their behaviors rely on the structure. The structural class, degree of hydroxylation, various substitutions and conjugations, and degree of polymerization all affect the chemical constitution of flavonoids [10]. Flavonoids also act as a secondary antioxidant defense system in plant tissues exposed to different abiotic and biotic stresses [11]. There is strong scientific evidence linking high flavonoid consumption to a variety of health benefits, including a lower risk of cancer and heart disease, protection against free radical damage, inhibition of tumor growth, and improved insulin production [12].

Research on the absorption and metabolism of flavonoids, especially flavonol, has increased significantly in the last few years. Research indicates that the absorption of flavonol conjugates is higher than that of the parent aglycone [13]. An association between higher amounts of dietary flavonol and slower cognitive decline but does not prove that flavonol directly causes a slower rate of cognitive decline. Benavente--García gave the relation between each structural factor of Citrus flavonoids and the anticancer, anti-inflammatory, and cardiovascular protection activity of Citrus flavonoids and their role in degenerative diseases [14].

Flavonoids can alter the activity of proteins during cell development [15]. The antibacterial activity of the compound as well as the reference antibiotic, ciprofloxacin was tested on Gram-negative multi-drug-resistant bacteria overexpressing active efflux pumps, and against methicillin-resistant strains of *Staphylococcus aureus* (MRSA) [16]. Even in middle age, promoting a higher consumption of some flavonoid-rich foods and drinks, such as tea, blueberries, red wine, and peppers, may reduce the risk of premature mortality [17]. Chromatography/mass spectrometry and fluorescence microimaging techniques findings offer new evidence on the inter- and intracellular distribution of stress-responsive on how flavonol may have performed a wide array of functional roles during the colonization of land by plants [18]. The two binding sites are involved in BSA–3HF interaction and the interaction is slightly positively cooperative with a similar binding constant [19]. Flavonol is hypothesized to reduce the risk of breast cancer through its effects on several biochemical pathways involved in carcinogenesis [20].

An attempt has been made to study the molecular geometry and molecular vibrational of the 3-Hydroxyflavone based on density functional theory due to their divergent usage. Molecular docking (Biochemical processes) studies using the Prothrombin (1A2C), Neutrophil collagenase (1A86), and Glutathione S-transferase P (18 GS) protein of Homo Sapiens with ligand 3-Hydroxyflavone are performed. The function of many enzymes is dependent on the tunnels and gates they include. The movement of ions, solvent molecules, and tiny molecules such as substrates and products into and out of the structure of the enzyme is controlled by gates, which reversibly flip between open and closed conformations. Molecular dynamics investigate the reaction of a biomolecular system to a perturbation. An antigenic protein's surface structure has a conformational epitope, which is made up of nearby amino acid residues that help in understanding the immune system.

2. Applied method

The calculations were performed by the DFT method on 11th Gen Intel(R) Core (TM) i5-1135G7 @ 2.40 GHz, 2419 MHz, 4 Core(s), 8 Logical Processor(s)z personal computer using Gaussian 09W program [21] package. Harmonic vibrational frequencies were calculated, the frequencies were scaled and the structure was optimized. We compute the vibrational frequencies and energies of optimized structures using the Lee-Yang-Parr (LYP) correlation function [22] and the gradient-corrected density functional theory [23] (DFT) with the three-parameter hybrid functional [24] (B3) for the exchange portion. The computer program VEDA 4 was used to calculate the potential energy distribution (PED), which optimizes the internal coordinate [25]. Initial optimization was done with the force field and then studied with partitioning schemes. Selected single-point energy analyses using the PES scan are conducted, and internal coordinates using Gauss view 5.0 [26]. Molecular Docking studies were carried out using the AutoDock suite [27]. The protein chosen was added with hydrogen (polar) by removing the water molecules. The Kollman charges were added and computed by Gasteiger. The input ligand through the torsion tree, root was detected and from the chosen torsion for the ligand the corresponding set was taken for active torsion. The protein and ligand as macromolecules in the grid are identified. From the PDBQT, both ligand and protein are generated and docked. The generated configuration from AutoDock as a docking engine, the output is taken from the executed file and discussed. Molecular Dynamics program dart in ubuntu 20.040 version Linux terminal with Linux command program tool (GUI) Gromacs-2022.5 and analyzed protein-ligand interaction using protein Glutathione **S-transferase P** with 3-Hydroxyflavone

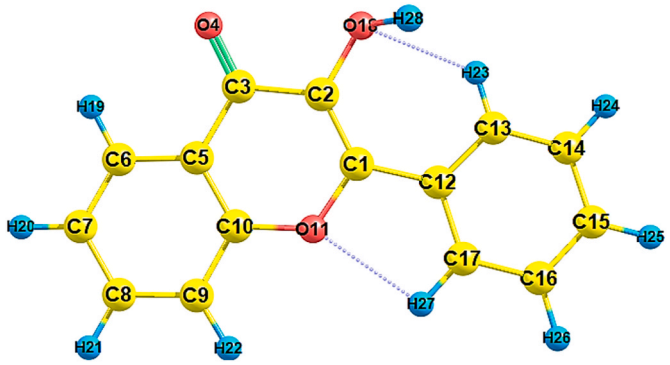

Fig. 1. Numbering system adopted in this study (3-Hydroxyflavone).

ligand [28].

3. Results and discussion

3.1. Molecular geometry

The Berny geometry optimization algorithm is implemented [29]. Convergence is tested against criteria such as maximum force component, root-mean-square force, maximum step component, and root-mean-square step. The optimized parameters are tabulated in Table 1 according to the molecule's atomic numbering in Fig. 1. The molecule is thought to have symmetry in the C1 point group. The exact experimental data of the geometrical parameter of 3-Hydroxyflavone is taken from Cornard [30]. A maximum number of the bond length and bond angle are well correlated to the experimental data. The shorter bond length of O18–H28 (0.96 Å) is due to stronger the bond. The bond length C1–C12(1.474 Å) bonded with O11, C2–C3(1.457 Å) bonded with O4, C3–C5(1.446 Å) bonded with O4 shows lowering of length in C1–O11(1.369 Å), C3–O4(1.232 Å) and C2–O18(1.357 Å). Because oxygen is an electronegative element, bonding electrons are more drawn to it.

3.2. Hydrogen bond

Indirectly, hydrogen bonding can be observed in protein crystallography. The bond is assumed to be a hydrogen bond if an appropriate acceptor-donor pair for a hydrogen bond is present within the right distance. In general, this distance is thought to range between 2.7 and 3.3, with 3.0 being the most typical number for hydrogen bonding between proteins and water. The closer the hydrogen bond is to correct geometry, the stronger the bond [31]. It is widely accepted that C–H … …. O hydrogen bonds play an important role in determining macromolecular conformation [32]. C–H … …. O interactions have the same tendency toward linearity as conventional H-bonds but are less sensitive to angular deformations [33]. In the present study C17–H27 … … …. O11 consists of an oxygen atom bonded to a hydrogen atom H27 forming hydrogen bond length 2.26 Å. The H28–O18 … … … H23 (hydroxyl group) which consists of an oxygen atom bonded to a hydrogen atom H23 forming a hydrogen bond length of 2.27 Å. This is due to the bond between the oxygen and the hydrogen being highly polar due to the high electronegativity of the oxygen atom The predicted hydrogen bond in dotted lines is shown in Fig. 1.

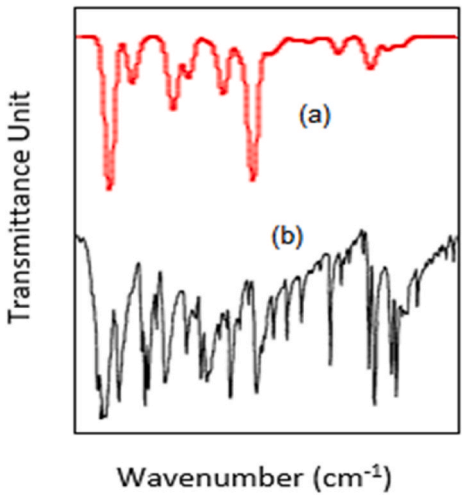

Fig. 3. IR (a) Calculated (b) Experimental spectra of 3-Hydroxyflavone.

3.3. Potential energy surface

Relaxed potential energy surface (PES) scans are frequently employed to comprehend reaction mechanisms, identify transition structures, investigate bond stability, and assess conformational flexibility [34]. The relaxed potential energy surface (PES) scan, which entails single-point energy evaluations over a rectangular grid including chosen internal coordinates is carried out. The number of steps and step size for each variable are 10°,20° … …. for dihedral angle, C1–C2–C12–C13 is performed. The two-fold hyperconjugation is shown

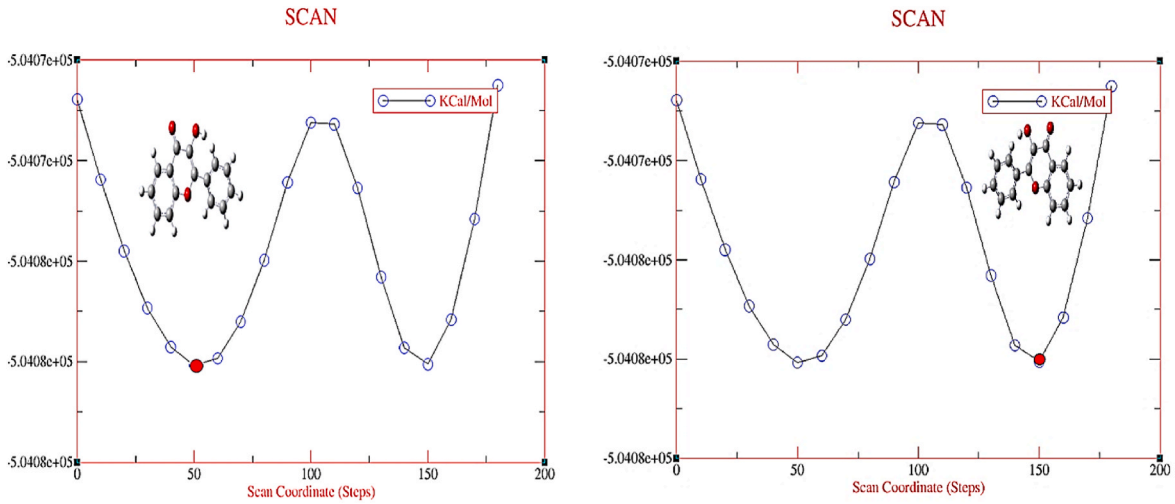

Fig. 2. Scan Coordinate for Dihedral angle C1–C2–C12–C13.

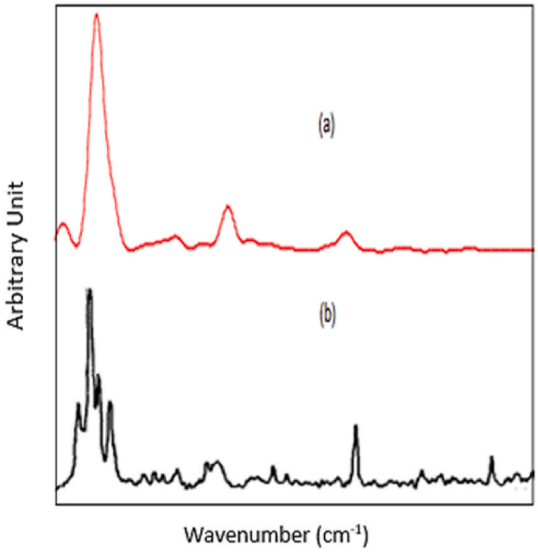

Fig. 4. Raman (a) Calculated (b) Experimental spectra of 3-Hydroxyflavone.

Table 2
Calculated and Vibrational wavenumber, measured IR and Raman band Positions (cm^{-1}) and assignments for 3-Hydroxyflavone.

Mode No.	Experimental		Scaled Frequencies[a]	Vibrational Assignments (PED%)
	FT-IR[b]	FT-Raman[b]		
11	1645	1648	1678	ν CO (38), ν C═O (10), ν OH (10), ν C–C (38)
12	1605	1600	1600	ν C═O (22), ν CC (61)
15	1570	1570	1566	ν C═O (15), δ OH (10), ν CC (11)
16	1545	1540	1558	ν C═O (37), δ OH (27), ν CC (30)
17	1475	1475	1477	ν CC (42), δ OH (10)
18	–	–	1455	ν CC (31), δ OH (10)
19	–	–	1451	ν CC (18), δ OH (10)
20	1435	1420	1431	ν CC (31), δ OH (28)
21	–	1370	1395	δ OH (20), ν CC (71)
22	–	1350	1331	δ OH (65), ν CC (23)
23	1310	1320	1313	ν CC (12), δ OH (39)
24	–	–	1286	ν CC (11), δ OH (25)
25	1270	1275	1273	ν CC (17), δ OH (15)

ν-stretching, δ-plane bending
[a] scaling factor: 0.961 for DFT (B3LYP/6-31G (d, p)).
[b] Ref: [30].

in Fig. 2 for dihedral angle C1–C2–C12–C13. When the atoms come closer, the energy becomes minimum and the minimum energy gives the most stable state of the system. The separation will represent the equilibrium point and the best separation. The minimum energy value was found at scan steps 50 and 150 with −504076 kcal/mol and all energy is shown in the XM-graph Fig. 2. The predicted change in energy was at −4.477881D-08 unit during the scan.

3.4. Vibrational assignment

3-Hydroxyflavone possesses 28 atoms with 78 normal modes, out of which major vibrational findings of the compound were carried out such as C–O, C═O, O–H, and C–C. The measured and calculated Infrared and Raman spectra of 3-Hydroxyflavone [30] taken for the comparison are shown in Figs. 3 and 4. The calculated frequencies from the B3LYP/6-31G (d, p) are greater than the results of the experiments, this is due to insufficient electrical correlation implementation hence it is adjusted with factors in this work. The scaled frequencies, Infrared, and Raman with their vibrational assessment along with potential energy distribution are given in Table 2. To analyze the IR and Raman spectra, the VEDA computer program optimizes the set of internal coordinates. As a result, the theoretical normal modes are represented by internal coordinates, providing users with a more intuitive understanding of molecular movements. Almost all of the theoretical data in the table correlates with experimental IR and Raman frequency.

The stretching frequency is reduced when a C═O bond is conjugated with a double bond or phenyl ring. The C–*O*–H in-plane bending falls in 1415 cm^{-1}. The C–O stretching at wavenumber 1240 cm^{-1} confirms our study at 1270 $cm^{-1}$and 1275 cm^{-1} as stretching C–C and in combination with in-plane bending of O–H. Usually, 1613 medium peak gives C–C skeletal vibrations, and C–C stretching also falls at 1605 cm^{-1},1600 cm^{-1}, and 1600 cm^{-1} in this study. Medium peak found at 1580–1578 cm^{-1} and 1545–1542 cm^{-1} shoulder peak shows C–O vibrations, IR 1570 cm^{-1}, Raman 1570 cm^{-1} and theoretical at 1566 cm^{-1} gives the C═O combined with O–H and C–C and also at 1545 cm^{-1}, 1540 cm^{-1}, 1558 cm^{-1} with stretching C═O in-plane bending O–H and stretching C–C. The weak peak at 1400 cm^{-1} and 1375 cm^{-1} gives O–H bending vibrations, and –C–O–H in-plane bending vibrations. Weak 1317 cm^{-1}, weak 1294–1292 cm^{-1}, weak 1271 cm^{-1}, and at 1227 cm^{-1} with strong peak showing C(O)–O stretching vibrations and –OH in-plane vibrations, 1157 cm^{-1} (sh) C–O stretching vibrations. The vibrations at the 1370 cm^{-1}, 1350 cm^{-1}, 1320 cm^{-1}, 1275 cm^{-1} in Raman, and 1310 cm^{-1},1270 cm^{-1} at IR almost correlate with the theoretical study showing in-plane bending and CC stretching.

3.5. Wave function

The computation of wave function overlaps for various wave function expansions, molecular orbitals, basis sets, and molecular geometries is done concurrently using a flexible formalism. The key conclusions are stated in a series of lemmas, corollaries, and theorems that are satisfied by the zeros of the real and imaginary sections of the wave functions on the real line. The wave function ψ may be positive, negative, or imaginary. [ψ]2 is known as probability density and determines the probability of finding an electron at a point within the atom. We run the wave function program output and parameters of the C5, C10, and O11 atoms and compared and confirmed molecular atoms six-membered and highlighted O2 in this both graph and 3-Hydroxyflavone is a combination of two benzene rings with heterocyclic pyrone structure shown in Fig. 5.

Electron Localization Function (ELF) is shown in Fig. 6 (a) the blue and especially dark blue regions exhibit a decrease of ELF in corresponding regions. This plot demonstrates that the electron localization decreases in the intermolecular contact regions during complex formation; this decrease may be a result of the Pauli repulsion effect in the shaded surface map with projection—input index of three atoms C5, C10, and O11. X/Y/Z of origin of the plane is x = −4.91778, y = −7.72252 z = 0.59021 Bohr, X/Y/Z of end of the plane is x = −0.4810, y = 7.6031 and z = −0.5016 Bohr. The minimum energy of ELF is 1.9304E-003 and the maximum energy of ELF is 0.9999.

Localized orbital locator (LOL) shown in Fig. 6 (b) and Color-filled map In this example we plot localized orbital locator (LOL) for an energetic compound, 3-Hydroxyflavone LOL is a popular function for revealing electron localization. The input file in this section is RB3LYP/6-31G (d, p) and atoms C5, C10, and O11 load it into Multiwfn. If it finds the objects in the exported image are truncated at their edges, you should select the high LOL-regions (red or orange color regions) that reveal the favorable delocalization path shown in Fig (b) X/Y/Z of origin of the plane x = −4.91778, y = −7.72252 and z = 0.59021 Bohr. X/Y/Z of end of the plane x = −0.45865, y = 7.68057, and z = −0.50714 Bohr and The minimum of LAL energy = 1.7487E-002 and the maximum of energy is 0.97615 color-filled map. The atoms type the Interaction region indicator (IRI) and Average local ionization energy (ALIE**).**

Average local ionization energy (ALIE**)** the result of ALIE C5, C10,

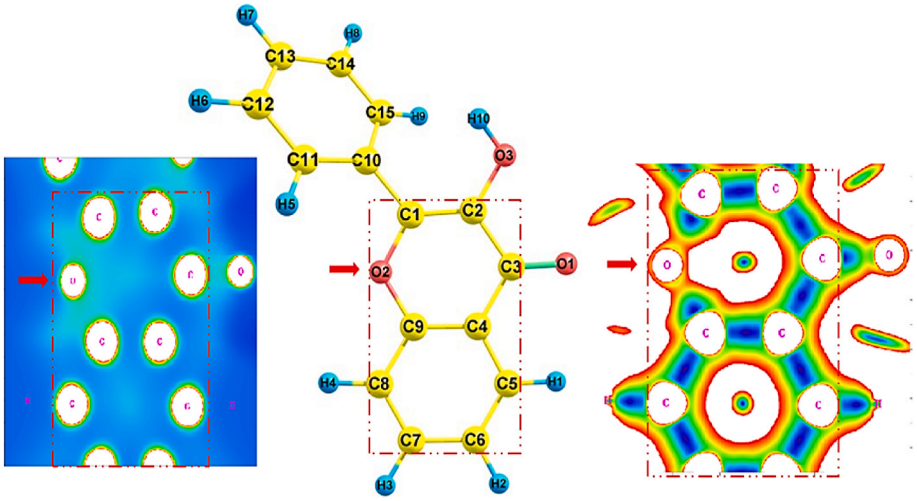

Fig. 5. IRI and Alice Structure with 3-Hydroxyflavone structure.

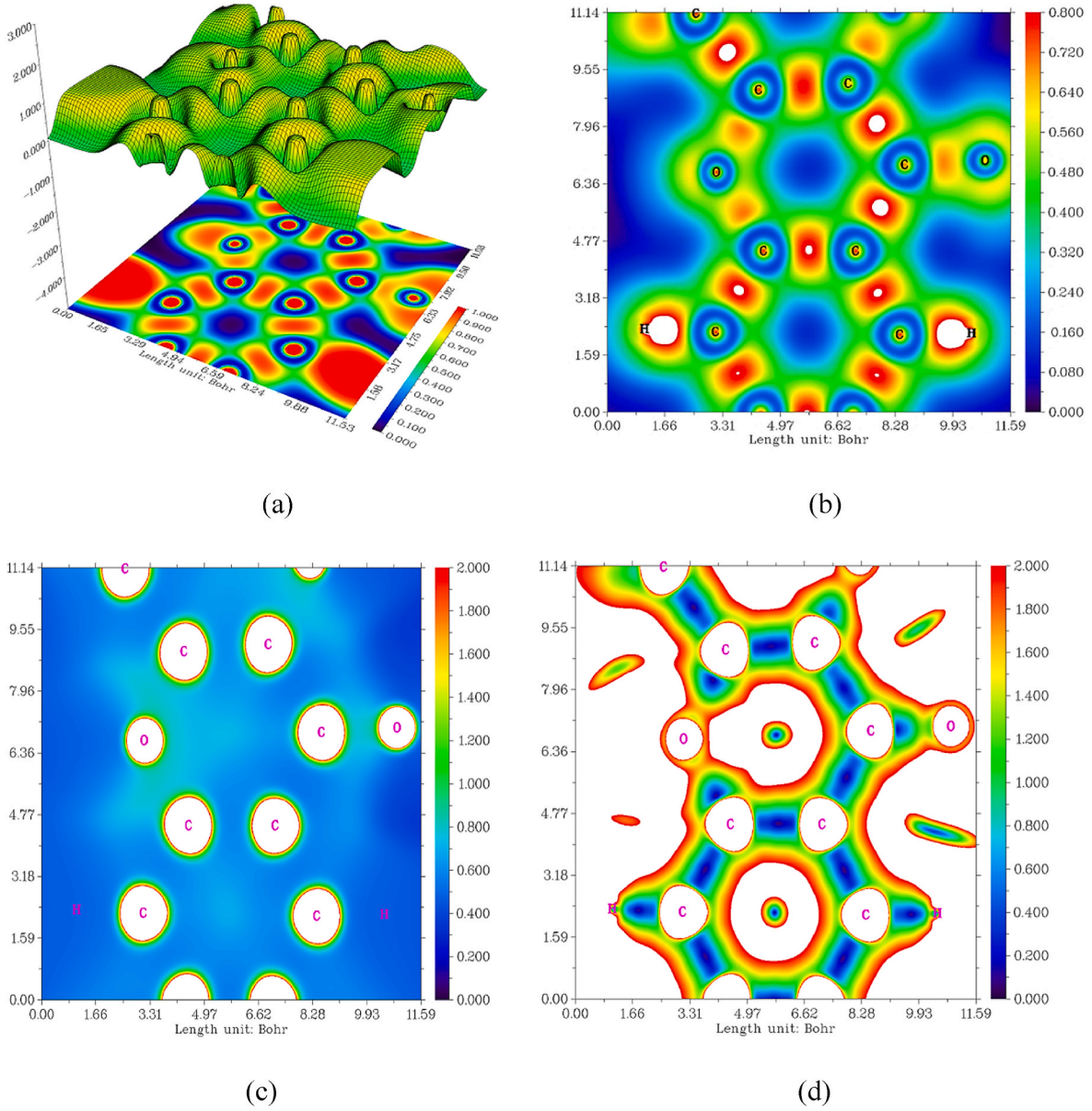

Fig. 6. Wave function Structures of 3-Hydroxyflavone (a) Electron Localization Function (ELF), (b) Localized orbital locator (LOL), (c) Average local ionization energy (ALIE), (d) Interaction region indicator (IRI).

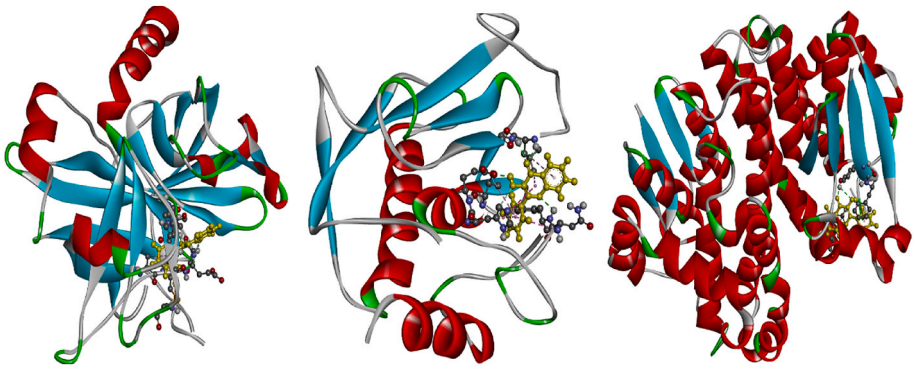

(a) 1A2C (b) 1A86 (c) 18GS

Fig. 7. 3D structural domains of Homo Sapiens with Ligand.

O11 X/Y/Z of origin of the plane is x = −4.91778 y = −7.72252 and Z = 0.59021 Bohr, X/Y/Z of end of the plane = x = −0.45865, y = 7.68057 and z = −0.50714 Bohr. The minimum energy of ionization energy is 0.34786, and the maximum ionization energy is 18.5133 observed in ALIE further details are shown in Fig. 6 (c).

Interaction region indicator (IRI) of Color-filled map this system is all nearly lying in this plane. The orange and green areas (IRI <1.0) in this map reveal the regions where notable chemical bond interaction and weak interaction occur. The regions with IRI >1.0 have either a large gradient of electron density or negligible electron density; they are not of chemical interest. IRI plane X/Y/Z origin is x = −4.91778,y = −7.72252 and z = 0.59021 Bohr, X/Y/Z of end of the plane is x = −0.45865, y = 7.68057 and z = −0.50714 Bohr, X/Y/Z of translation vector one is x = −0.02712,x = 0.05141 and z = −0.00351 Bohr, Norm = 0.05823, X/Y/Z of translation vector two is x = 0.04953,y = 0.02599 and z = −0.00200 Bohr, Norm = 0.05597. The minimum IRI is 2.156343E-005 and the maximum IRI is 0.690523 observed details shown in Fig. 6 (d). We present a simple and efficient embedding scheme for the wave-function-based calculation of the energies of local excitations in large systems. The IRI, reveals the notable chemical bond interaction and weak interactions [35].

3.6. Molecular docking

Molecular docking has grown to be a significant step in the drug discovery process, it helps us to understand how ligands interact with enzymes. Good target identification and validation increase confidence in the target-disease link and allow us to investigate whether target modification will result in mechanism-based side effects [36]. Pharmacophore requires knowledge of either the active location of the target receptor or the active ligands. To identify the chemical characteristics that a group of active drugs have and that appear to be often crucial for receptor engagement, use common feature analysis [37]. To determine the exact functional region of the protein, active site prediction is required. Fig. 7 expresses the computational method to identify 3D structural domains and active site residues by using the **Prothrombin** (1A2C) shown in Fig. 7(a), **Neutrophil collagenase** (1A86) shown in Fig. 7(b), **Glutathione S-transferase P** (18 GS) shown in Fig. 7(c) the protein of Homo Sapiens with Ligand 3-Hydroxyflavone. Active site dimensions were set as grid size of center XYZ axis to dock the ligand with 8 maximum exhaustiveness used for each protein. Charges were assigned to protein and ligand structures for docking Analysis with UFF 318 (kcal/mol). The corresponding grid size is tabulated in Tables 3–5 which gives the best binding affinity found for the Protein **Glutathione**

Table 3
Binding affinity, Grid of 3-Hydroxyflavone with 1A2C protein.

Ligand: 3-Hydroxyflavone UFF: 318 kcal/mol	Best Ligand Pose Kcal/mol	Exhaustiveness = 8 Grid center: x = 14.5264, y = −5.5587, z = 18.2368							
Protein: 1A2C	Final Pose	1	2	3	4	5	6	7	8
Binding Affinity Kcal/mol	−7.00	−6.90	−6.70	−6.50	−6.50	−6.40	−6.30	−6.30	−6.10
RMSD/Upper Bound (Å)	0.00	2.24	3.70	5.67	14.01	22.00	36.70	25.30	13.69
RMSD/Lower Bound (Å)	0.00	1.65	1.83	2.92	12.88	20.28	35.58	22.54	12.98

Table 4
Binding affinity, Grid of 3-Hydroxyflavone with 1A86 protein.

Ligand: 3-Hydroxyflavone UFF: 318 (Kcal/mol)	Best Ligand Pose Kcal/mol	Exhaustiveness = 8 Grid center: x = 20.7061, y = 58.92, z = 52.0281							
Protein: 1A86	Final Pose	1	2	3	4	5	6	7	8
Binding Affinity Kcal/mol	−7.30	−6.10	−6.00	−5.90	−5.90	−5.80	−5.70	−5.70	−5.70
RMSD/Upper Bound (Å)	0.00	5.51	2.70	24.50	4.62	24.66	25.93	6.32	7.17
RMSD/Lower Bound (Å)	0.00	1.30	1.61	23.55	3.09	23.47	23.91	3.78	4.61

Table 5
Binding affinity, Grid of 3-Hydroxyflavone with 18 GS protein.

Ligand: 3-Hydroxyflavone UFF: 318 (Kcal/mol)	Best Ligand Pose Kcal/mol	Exhaustiveness = 8 Grid center: x = 19.4216, y = 55.7432, z = 50.5905							
Protein: 18 GS	Final Pose	1	2	3	4	5	6	7	8
Binding Affinity Kcal/mol	−8.10	−8.10	−7.80	−7.80	−7.30	−7.20	−7.00	−7.00	−7.00
RMSD/Upper Bound (Å)	0.00	6.25	30.92	30.03	31.04	29.90	30.46	29.69	29.72
RMSD/Lower Bound (Å)	0.00	2.11	28.67	29.02	28.80	28.98	28.28	28.71	28.75

S-transferase P (18 GS) at −8.10 kcal/mol. The most typical method of assessing the accuracy of the docking geometry is to calculate the Root Mean Square Deviation (RMSD) of the ligand from its reference position in the response complex following the ideal superimposition of the receptor molecules [38]. The calculated RMSD value shows the docking pose distance, the minimum RMSD i.e., lesser than 2 Å is fairly good [39], and it varies from 2.11 Å - 1.30 Å.

From the Ligplot shown in Fig. 8(a), the distance of 2.71 Å confirms the interaction between the ligand and the **Glutathione S-transferase P** (18 GS) protein. Fig. 8(b) shows the hydrogen bond interaction between the ligand and the **Glutathione S-transferase P** (18 GS) protein; the pink region is the donor with green as the acceptor. Ligand surface Path and Posses volume surface binding of 18 GS with 3-Hydroxy flavone complex. It was analyzed Several docking methods that best pose Volume 112.13 $Å^2$ Surface 218.06 $Å^2$ Depth 8.2 Å and the path of ligand surface highlighted visually in color more binding surface details shown in Fig. 8(c).

3.7. Reaction between glutathione S-transfers P and ligand

Interaction is visualized in the DSV (Discovery Studio Visualizer) software tool [40]. Fig. 9 shows the 3D and 2D structural domains of **Glutathione S-transferase P** (18 GS) with ligand, interactions such as favorable atoms interaction group interacting with B: PHE:7 as hydrophobic of Pi-Hydrophobic observed Pi-Pi stacked, favorable interacting atoms groups interacting with B: TYR:107 as hydrogen bond of Pi donor hydrogen sbond, in particular B: TYR:6 is interacting with favorable atoms interaction group as hydrogen bond observed in a conventional hydrogen bond with 1.91 Å are also found participating during the reaction.

Fig. 10 (a) and 10(b), explain the estimation of solvent-accessible surface area, with maximum availability of the molecule to the solvent

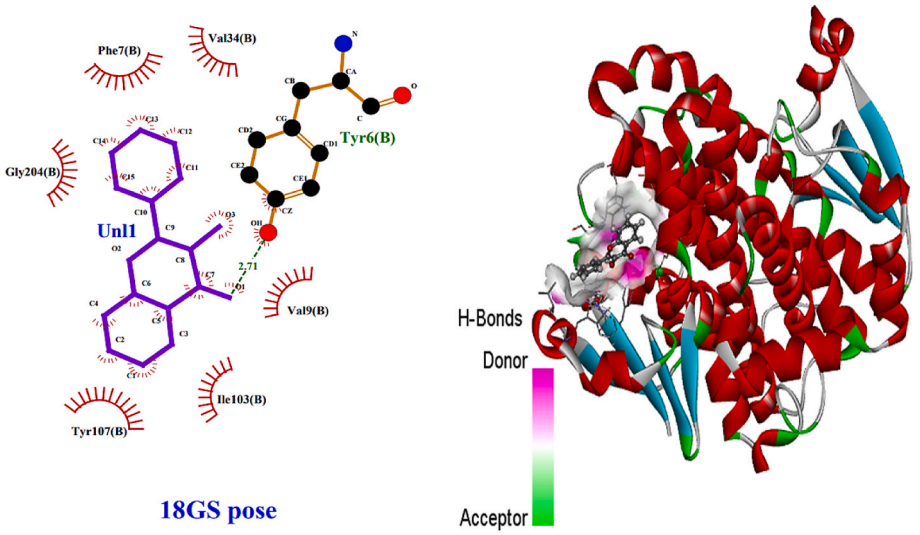

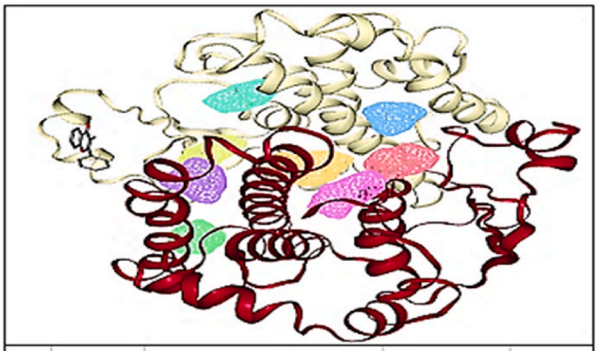

	Name	Volume [Å³]	Surface [Å²]	Depth [Å]
	P_1	112.13	218.06	8.2
	P_2	73.73	240.7	6.65
	P_3	70.14	176.59	5.66
	P_4	67.58	193.33	7.02
	P_5	66.56	221.94	6.65
	P_6	65.54	194.09	6.79
	P_7	64.51	169.56	7.63
	P_8	64.51	165.51	7.63

(c)

Fig. 8. (a) LigPlot 18 GS complex (b) Hydrogen bond of 18 GS with Ligand. (c) Ligand surface Path and Posses value of 18 GS with 3-Hydroxyflavone complex.

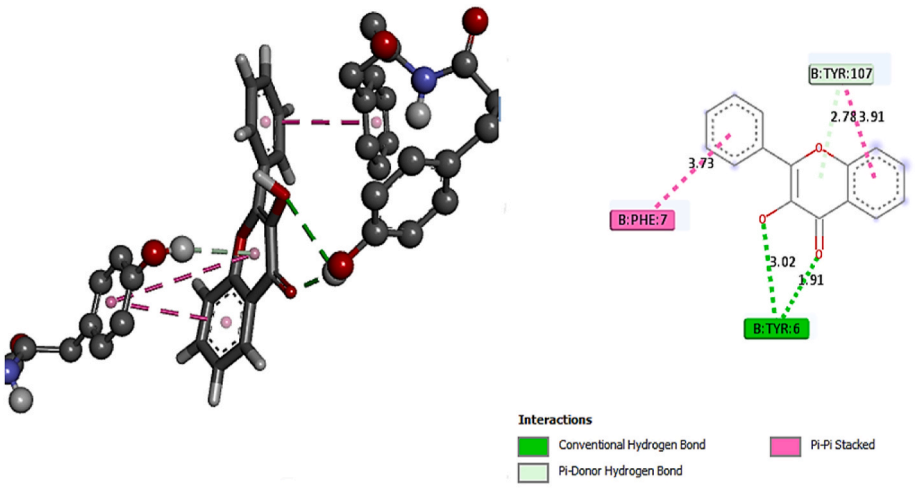

Fig. 9. 3D and 2D structural domains of 18 GS with Ligand.

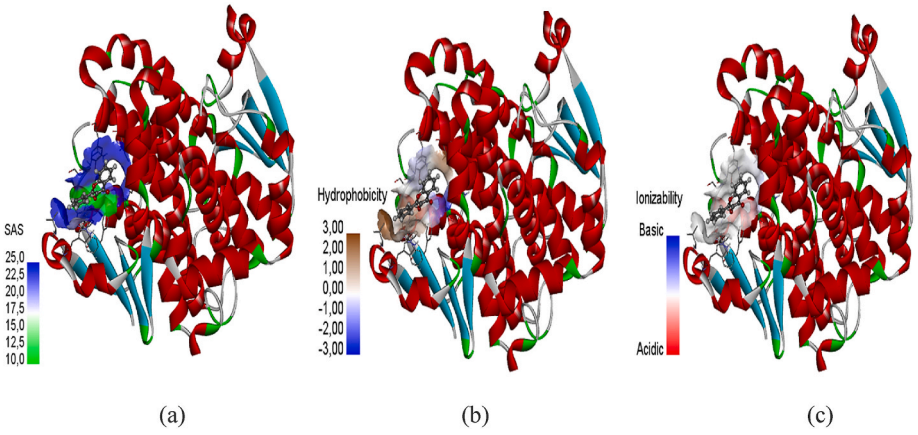

Fig. 10. (a) SAS, (b) Hydrophobicity, and (c) Interpolated charge of 18 GS with Ligand.

and also the hydrophobicity of the compound, associated with the existence of nonpolar groups or molecules in an aquatic environment resulting from water's propensity to reject nonpolar molecules [41]. The interpolated charge of the binding pocket residues is given (see Fig. 10 (c)).

3.7.1. Molecular dynamics glutathione S-transferase P with 3-hydroxyflavone

MD simulations are uniquely suited for examining the structures of membrane-associated protein-ligand complexes with atomistic detail [42]. With zenith widgets, the workflow gives the user information while requiring the least amount of interaction in terms of energy conservation, simulation time, and output file name. After obtaining input files and settings, it starts MD simulations (energy minimization, NVT, NPT, and MD), which require commands to a line-based protocol. Proteins can fold quickly because they have funnel-shaped energy landscapes that progressively direct the protein towards increasingly low energies as it folds [43]. The MD modeling of biomolecular systems is characterized by three major key structural metrics: Rg, RMSD, and RMSF. The GROMACS module calculates the potential energy, gmx rms, gmx gyrate, gmx hydrogen bond, gmx rmsf. The Rg, RMSF, Hydrogen Bonds, and Protein with Ligand Interaction are described in Table 6. In comparison to the reference beginning structure, the RMSD calculates the average distance between atoms in a structure at each given point throughout the simulation. As a result, it's employed to examine the general time-dependent structural deviation or degree of similarity

Table 6
MD program parameters analysis details.

Gmx make_ndx em.gro				Gmx Topology details
0	System	45805	atoms	Structure file Reading
1	Protein	6536	atoms	Protein A & B Chain: 416 Protein
2	Protein-H	3262	atoms	residues
3	C-alpha	416	atoms	LIG: 1 Other residues
4	Backbone	1248	atoms	SOL: 13079 Water residues
				NA: 4 Ion residues
5	MainChain	1662	atoms	**Gmx Energy Minimization details**
6	MainChain + Cb	2042	atoms	writing lowest energy coordinates.
7	MainChain + H	2062	atoms	Energy Minimization Values
8	SideChain	4474	atoms	Potential Energy = −6.6259162e+05
9	SideChain-H	1600	atoms	Maximum force = 9.7185706e+02
10	Prot-Masses	6536	atoms	on atom 6549
				Norm of force = 2.1461936e+01
11	non-Protein	39269	atoms	**Gmx mdrun nvt and npt details**
12	Other	28	atoms	Using 1 MPI thread, Using 8 OpenMP
13	LIG	28	atoms	threads starting mdrun 'Protein in
14	NA	4	atoms	water'
				50000 steps, 100.0 ps.
15	Water	39237	atoms	**Gmx md Reading file ran details**
16	SOL	39237	atoms	Using 1 MPI thread
17	non-Water	6568	atoms	Using 8 OpenMP threads starting
18	Ion	4	atoms	mdrun 'Protein in water'
19	Water_and_ions	39241	atoms	5000000 steps, 10000.0 ps.

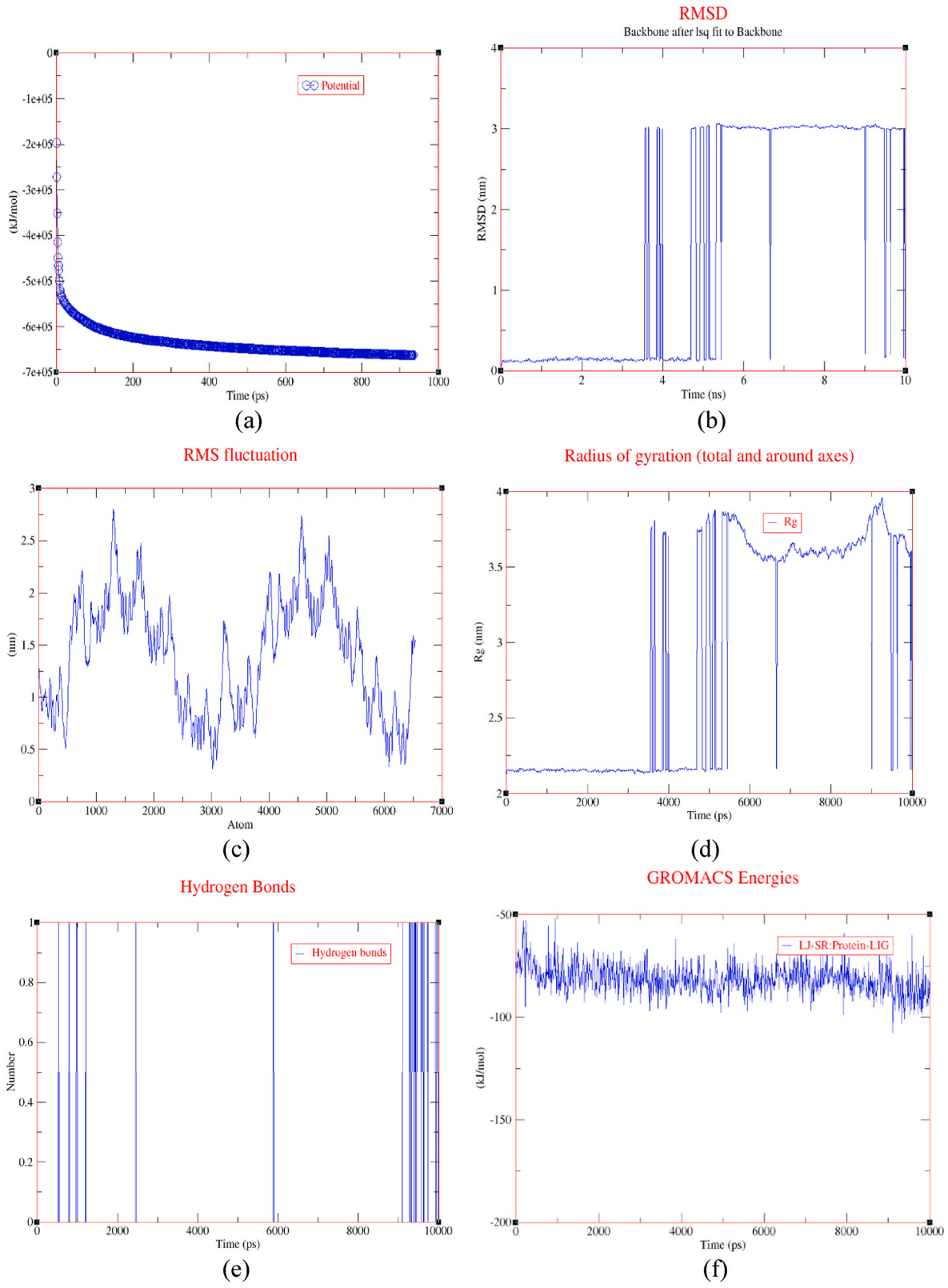

Fig. 11. (a) Potential Energy (b) Root-mean-square deviation **(c)** Root-mean-square fluctuation (d) Radius of gyration.

among the structures that the trajectory records. The RMSD plot of the protein under simulation (or the ligand in the case of a protein-ligand complex) is produced as xvg files by the Linux command with XM-grace software (Grace Home (weizmann.ac.il)). The average atomic or residue-level variations are measured by the RMSF, a standard mobility metric that, like the RMSD, measures the local fluctuations or flexibility inside a biomolecule during simulation details is shown in xm-graph in Fig. 11 RMSF sheds light on the dynamic areas of proteins, such as flexible loops, and can highlight the significance of particular residues in conformational shifts or interactions between proteins and

Table 7
MD xvg files output parameters.

Molecular Dynamics XVG -Data by XM-Graph				
Energy minimization (potential Energy)				
XM-Graph	**Energy**	**ST. Value**	**Mid Value**	**End Value**
X- axis	Time (ps)	0.000000	435.000000	935.000000
Y-axis	(kJ/mol)	−196480.875000	−644659.937500	−662591.625000
Root-mean-square deviation				
X- axis	Time (ns)	0.0000000	5.0000000	10.0000000
Y-axis	RMSD (nm)	0.0300322	3.0131850	3.0018547
Root-mean-square fluctuation				
X- axis	Atom	1	3187	6534
Y-axis	nm	1.2722	1.1966	1.5460
Radius of gyration				
X- axis	Time (ps)	0.00000	4720	10000
Y-axis	Rg (nm)	2.11037	3.74543	3.58624
Y-axis	Rg\sX\N	1.85794	3.55286	3.40542
Y-axis	Rg\sY\N	1.54203	1.67736	1.59973
Y-axis	Rg\sZ\N	1.75430	3.55249	3.40091
Hydrogen Bond Interaction				
X- axis	Time (ps)	0.0000000	4910	10000
Y-axis	Number	0.0000000	0.0000000	1
Y-axis	Pairs within 0.35 nm	0.0000000	2	0.0000000
Protein and Ligand Interaction (LJ-SR: Protein-LIG)				
X- axis	Time (ps)	0.00000	4750.000000	10000.000000
Y-axis	(kJ/mol)	−72.928680	−94.700089	−78.348221

LJ-SR: Protein-LIG = Average Interaction Energy −81.4899, Err. Est. = 1.3, RMSD = 7.16107, Tot-Drift = −7.64253 (kJ/mol).

ligands. A popular metric for assessing how compact protein molecules is in Rg. Lower values of Rg correspond to a more folded or compact structure, while higher values indicate more stretched or flexible conformations during simulation. In molecular dynamics (MD) simulations of biomolecules, hydrogen bond (HB) analysis is frequently employed to explore and comprehend protein structure, folding, function, and ligand binding, among other biomolecular interactions. The GROMACS protein-ligand interaction module and the gmx hbond are used to calculate h-bonds (Protein group 1 with ligand group 13) and the pairing distance in 0.35 nm. The numbers of intra- and intermolecular hydrogen bonds are computed and shown as a function of simulation time, depending on the kind of system [44]. MD xvg files support with XM-Graph software outputs are described in Tables 6 and 7 and shown details graph in separated modules mention in Fig. 11 (a to f). This gives the non-bonded interaction between the protein and the ligand. From the interaction, it is observed that the Coulombic and Lennard-Jones (short range energy) is −81.4899 kJ/mol.

3.8. Tunnels-pores in glutathione S-transferase P

The MOLE online server web interface's ability to see and analyze tunnels and pores allows for simple, online interaction with biomacromolecule investigation. The automatic transmembrane channel calculation on the quickest list of ligands for transport analysis and tunnel identification is on the MOLE online server. The automatic assistance techniques let users configure the calculation to produce biologically pertinent findings. It is possible to compute and visualize the detected tunnels' characteristics, energy profiles, and ligand-passage trajectories. LogD and LogP The partition coefficient, P, measures how differently a substance dissolves in two immiscible liquids. Octan-1-ol/water is the most often utilized solvent system. When a substance is neutral or only exists in one form, the partition coefficient serves as a description of its lipophilicity. We discuss the CHANNEL algorithm, which locates, characterizes, and displays tunnels or pores in proteins automatically [45].

Large collections of genuine proteins are analyzed using the method, which has had its accuracy tested on a manufactured set of proteins. The verification set includes proteins that have pores that were produced intentionally and have known route and breadth profiles.

Partition coefficient formula:

$$logp = log_{10}(partition\ coefficient) partition\ coefficient, p = \frac{[compound]octanol}{[compound]water}$$

Given that it measures the pH-dependent differential solubility of all species in the octanol/water system of the partition coefficient, the descriptor LogP = , which denotes a 10:1 ratio between Organic - Aqueous distribution coefficient, is the proper one to use for ionizable chemicals Distribution-coefficient-formula:

$$Distribution\ coefficient, D = \frac{\sum[Microspecies]octanol}{\sum[Microspecies]water}$$

Understanding the behavior of chemicals in actual structures is made easier by molecular physical characteristics. We can assess and predict the likely behavior of a compound using the values of molecular physical properties such as length, the radius of the channel bottleneck, the average hydropathy index, charge, the average of the lining amino acid polarity, the average mutability index, the average hydropathy index, logP (lipophilicity octanol/water partition), logD (lipophilicity octanol/water distribution), logS (water solubility), and ionizable. Detail in Table 8.

Tunnel analysis 1 (T2C1), Length of the channel 26 Å, Radius of channel bottleneck 1.5 Å, Average hydropathy index −3.05, Charge −2.0, Average of lining amino acid polarity 29.34, Average of mutability index 92, Lipophilicity octanol/water partition(logP) −0.1, Lipophilicity octanol/water distribution(logD) −1.52, Water solubility (logS) 1.29 and ionizable residues = 8.

Tunnels analysis 2. (T3C1) Length of the channel 26.8 Å, Radius of channel bottleneck 1.5 Å, Average hydropathy index −3.25, Charge −3.0, Average of lining amino acid polarity 25.86 Average of mutability index 80, Lipophilicity octanol/water partition(logP) 0.1, Lipophilicity octanol/water distribution(logD) −1.31, Water solubility(logS) 1.08 and ionizable residues = 7.

Tunnels analysis 3. (T4C1) Length of the channel 26.9 Å, Radius of channel bottleneck 1.5 Å, Average hydropathy index −3.19, Charge 2.0, Average of lining amino acid polarity 25.58, Average of mutability index 82, Lipophilicity octanol/water partition(logP) −0.0, Lipophilicity octanol/water distribution(logD) −1.26, Water solubility(logS) 1.06 and ionizable residues = 6.

Tunnels analysis 4. (T5C1) Length of the channel 32.3 Å, Radius of channel bottleneck 1.5 Å, Average hydropathy index −3.13, Charge

Table 8
Tunnels parameters analysis.

Tunnels Parameters										
Tunnels	Length	Bottle Neck	Hydropathy	Charge	Polarity	Mutability	logP	logD	logS	Ionizable
T2C1	26 Å	1.5 Å	−3.05	−2	29.34	92	−0.1	−1.52	1.29	8
T3C1	26.8 Å	1.5 Å	−3.25	−3	25.86	80	−0.1	−1.31	1.08	7
T4C1	26.9 Å	1.5 Å	−3.19	−2	25.58	82	−0	−1.26	1.06	6
T5C1	32.3 Å	1.5 Å	−3.13	−1	22.89	82	−0.1	−1.17	0.97	9
T6C2	19.6 Å	0.8 Å	−0.4	1	3.27	73	−0.2	−0.2	0.12	1
T7C3	14.9 Å	0.8 Å	−0.45	0	2.61	72	−0.1	−0.08	0.01	N/A
T8C4	11.4 Å	1.2 Å	−3.61	2	29.18	76	0.02	−1.27	0.82	2
T9C6	7.8 Å	1.6 Å	−0.89	0	25.39	77	0.92	−0.38	0.41	2

−1.0, Average of lining amino acid polarity 22.89, Average of mutability index 82, Lipophilicity octanol/water partition(logP) −0.1, Lipophilicity octanol/water distribution(logD) −1.17, Water solubility (logS) 0.97 Å and ionizable residues = 9.

Tunnels analysis 5. (T6C2) length of the channel is 19.6 Å, the Radius of the channel bottleneck is 0.8 Å, the Average hydropathy index is −0.4, the Charge is 1.0, the Average lining amino acid polarity is 3.27, the Average mutability index is 73, Lipophilicity octanol/water partition (logP) −0.2, Lipophilicity octanol/water distribution(logD) −0.2, Water solubility(logS) 0.12 and ionizable residues = 1.

Tunnels analysis 6. (T7C3) length of the channel 14.9 Å, Radius of channel bottleneck 0.8 Å, Average hydropathy index −0.45, Charge 0.0, Average of lining amino acid polarity 2.61, Average mutability index is 72, Lipophilicity octanol/water partition(logP) −0.08, Lipophilicity octanol/water distribution(logD) −0.01, Water solubility(logS) N/A and ionizable residues = 2.

Tunnels analysis 7. (T8C4) length of the channel 11.4 Å, Radius of channel bottleneck 1.2 Å, Average hydropathy index −3.61, Charge 2.0, Average of lining amino acid polarity 29.18, Average mutability index is 76, Lipophilicity octanol/water partition(logP) 0.02, Lipophilicity octanol/water distribution(logD) −1.27, Water solubility(logS) 0.82 and ionizable residues = 2.

Tunnels analysis 8. (T9C6) length of the channel 7.8 Å, Radius of channel bottleneck 1.6 Å, Average hydropathy index −0.89, Charge 0.0, Average of lining amino acid polarity 25.39, Average mutability index is 77, Lipophilicity octanol/water partition(logP) −0.92, Lipophilicity octanol/water distribution(logD) −0.38, Water solubility(logS) 0.41 and ionizable residues = 2. Further details are shown in Table 8 and shown in Fig. 12 (a, b)

3.8.1. *Pores analysis*

PFPs, which target membranes by creating channels through them, are recognized as significant agents in immunity and infection. In the three-dimensional (3D) architectures of proteins, surface pockets, cavities, and tunnels perform crucial functional roles that support enzyme catalysis, ligand binding, and the transport of ions or small molecules across biomembranes [46]. To do this, they switch from a form that is soluble in water to one that can be introduced into membranes. PFPs are arranged into supramolecular transmembrane complexes that perforate membranes via a multi-step process that includes membrane insertion, protein oligomerization, and eventually pore formation. Pores observed are volume 1 = 11303 Å, volume 2 = 1730 Å, volume 3 = 1495 Å, volume 4 = 659 Å, volume 5 = 395 Å, volume 6 = 246 Å, volume 7 = 210 Å, volume 8 = 127 Å details shown Fig. 13 Pores parameters are observed Radius 1,2,3,4,5,6 and 7 are 1.50,1.71,1.70,1.71,2.26,1.88 and 1.71. This Free R is 2.22, 2.78, 2.79, 2.78, 5.32,188 and 1.72. The Length is 27.2, 31.9, 33.2, 36.9, 42.8, 54.8 and 74.4. Hydropathy is −0.21, 1.23, −0.68, −1.12, −1.44, −1.18 and −1.14. Hydrophobicity is 0.45, −0.23, 0.16, −0.23, −0.08, −0.06 and −0.26. Polar is 9.6, 23.7, 17.3, 23.4, 12.8, 13.4 and 23.3. Rel. Mut is 80, 77, 71,77,81,81, and 82 Further details are clearly shown in Fig. 13 (a, b, & c).

The "pore criterion," which is a requirement imposed by this mode, states that the endpoints of the pore must be separated from one another by a distance greater than the average length of the channels that created the pore. The same criteria used to remove identical holes from channels in Fig. 13(c) are applied to all modes.

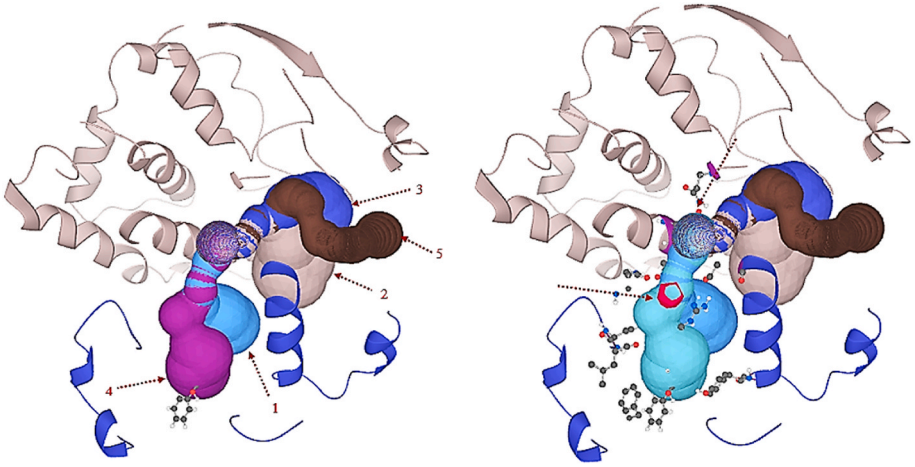

(a) (b)

Fig. 12. (a) tunnels structure, (b) layer and lining structure.

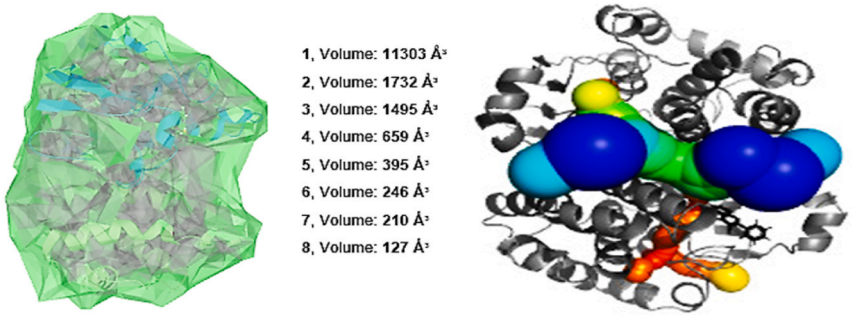

(a)

Pores

	Radius	Free R	Length	HPathy	HPhob	Polar	Rel Mut	Residue type						
1	1.50	2.33	27.2	-0.21	0.45	9.6	80	3	1	2	6	4	0	0
2	1.71	2.78	31.9	-1.23	-0.23	23.7	77	2	4	2	2	0	0	2
3	1.70	2.79	33.2	-0.68	0.16	17.3	71	2	4	1	3	3	2	2
4	1.71	2.78	36.9	-1.12	-0.23	23.4	77	3	4	2	2	0	0	2
5	2.26	5.32	42.8	-1.44	-0.08	12.8	81	3	0	2	3	2	0	0
6	1.88	1.88	54.8	-1.18	-0.06	13.4	81	2	1	4	4	3	2	0
7	1.71	2.78	74.4	-1.44	-0.26	23.3	82	5	5	6	4	1	0	2

(b)

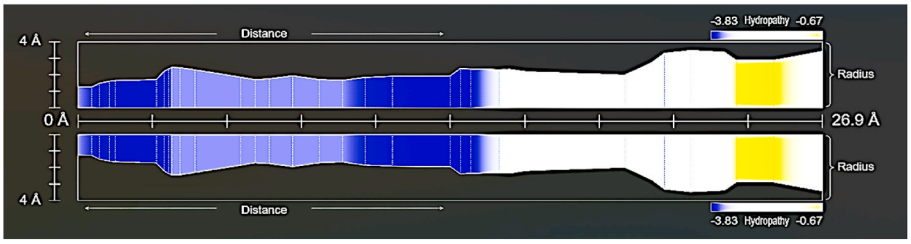

(c)

Fig. 13. (a) pores with cavity volume (b) pores parameters (c) channel view.

3.9. Epitope analysis in 18 GS protein with 3-hydroxyflavone complex

The epitope technique was designed as an online tool to evaluate the effectiveness of the approach's performance on linear and discontinuous epitopes (Ellipro) known from the structures of antibody-protein complexes. Chain A observed first linear epitope group has nine peptide residues in the group and a score of 0.747, the second linear epitope group has twenty-five peptide residues in the group and a score of 0.745, the third linear epitope group has sixteen peptide residues and a score 0.704, fourth linear epitope group has maximum twenty-nine peptide residue and score 0.704, fifth linear epitopes group has minimum five peptide residues and score 0.508, Chain B linear groups details also

Table 9
Expected linear Epitope(s).

Linear Epitope						
No	Chain	Start	End	Peptide	Number of Residues	Score
1	A	133	141	SQNQGGKTF	9	0.747
2	A	21	46	ADQGQSWKEEVVTVETWQEGSLKASC	25	0.745
3	A	162	177	EVLAPGCLDAFPLLSA	16	0.704
4	A	180	208	GRLSARPKLKAFLASPEYVNLPINGNGKQ	29	0.704
5	A	143	147	VGDQI	5	0.508
6	B	21	46	ADQGQSWKEEVVTVETWQEGSLKASC	26	0.749
7	B	133	141	SQNQGGKTF	9	0.724
8	B	162	177	EVLAPGCLDAFPLLSA	16	0.713
9	B	180	208	GRLSARPKLKAFLASPEYVNLPINGNGKQ	29	0.706
10	B	143	147	VGDQI	5	0.508

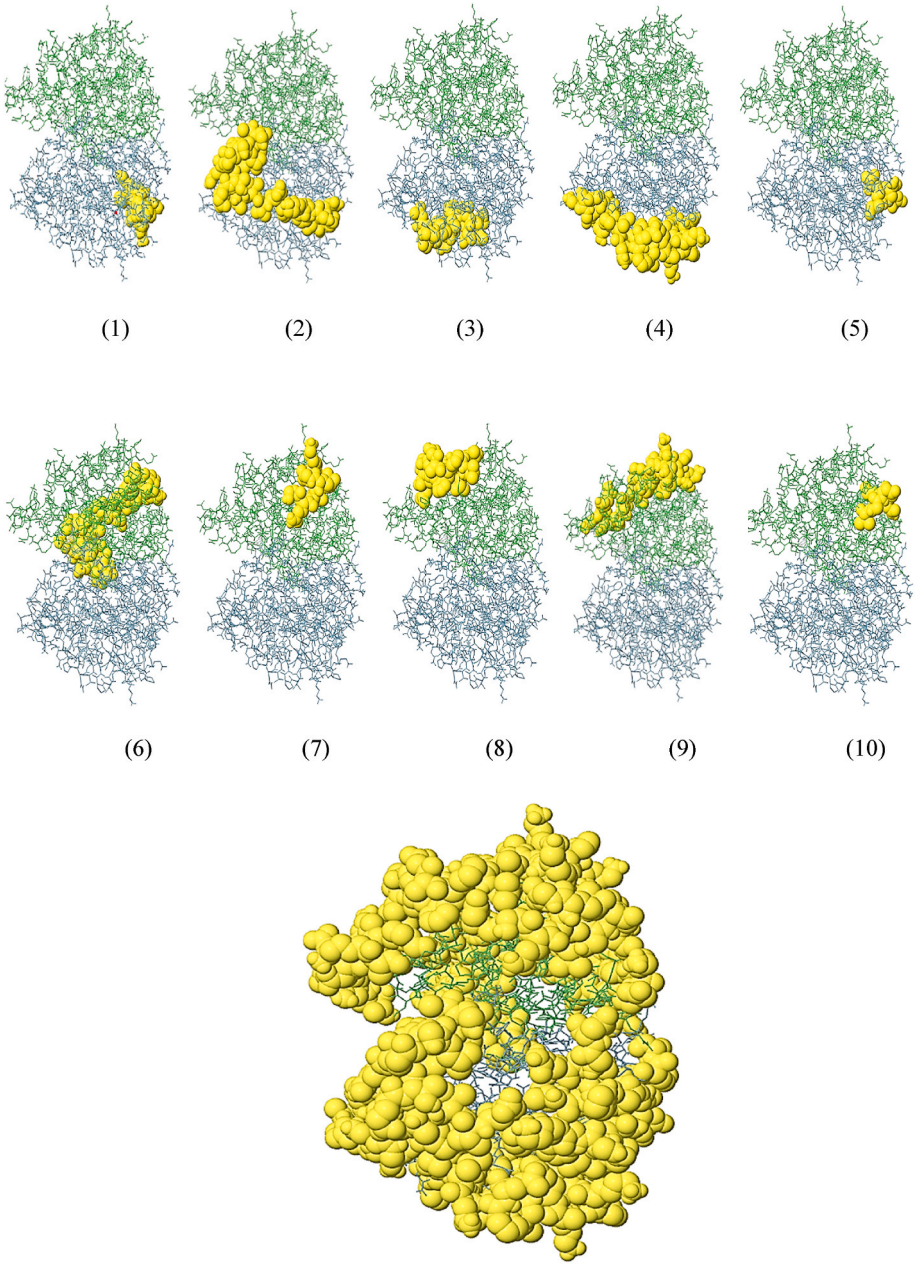

Fig. 14. (1–10) Peptide residues Epitope complementary binding with antigen (11) Peptide -JSmol Rendered PDB structures.

observed as sixth linear epitope was twenty-six residues and score 0.749, seventh linear epitopes group has nine peptide residues and score 0.724, Eighth linear epitope group has 16 peptide residues and score 0.713, Nineth linear epitope group has maximum twenty-nine peptide residues and score 0.706, and last tenth linear epitope group has minimum five peptide residues. This observation of the A and B protein chains has concluded the maximum effective score of 0.749 and twenty-six peptides. Additional information is provided regarding the B-Chain group peptide residues epitope complementary binding with antigen in this protein structure in Table 9 and shown in Fig. 14.

Discontinued epitope details of Chanin B and Chain A mentioned in Table 9. The score of B chain residues is 0.744 and Chain A residues score 0.743. Here, we introduce ElliPro, an online application that applies Thornton's method and uses a residue clustering algorithm, the MODELLER program, and the Jmol to predict and visualize antibody epitopes in a certain protein sequence or structure. the viewer is shown in Fig. 14. ElliPro has been evaluated on a benchmark dataset of discontinuous epitopes deduced from antibody-protein complexes' three-dimensional (3D) structures. Compared to 10 various structure-based methods for epitope prediction. A peptide bond is shaped at the molecular level by a dehydration synthesis or reaction. This process, which regularly happens between amino acids, is sometimes referred to as a condensation reaction. An epitope, also known as an antigenic determinant, is a region of an alien protein, or antigen that might elicit an immune response. An antigen's "epitope," or portion, binds to a specific antigen receptor on a B cell's surface. The building of peptide molecules are two or more amino acids connected by the synthesis of amides, which attach each amino acid to the carboxyl group and the next amino group. An epitope is typically 5–8 amino acids long, although peptides of 15–20 amino acids are frequently used. Therefore, an antibody response that recognizes multiple epitopes may, in theory, be induced by a peptide of 15–20 amino acids.

The chemical interaction between the carbon and nitrogen atoms in each amide group is known as a peptide bond. It is known that partial or

Table 10
Expected discontinuous Epitope(s).

No	Discontinuous Epitope	Score
Chain "B"	B:P1, B:Y2, B:T3, B:P8, B:V9, B:R10, B:A21, B:D22, B:Q23, B:G24, B:Q25, B:S26, B:W27, B:K28, B:E29, B:E30, B:V31, B:V32, B:T33, B:V34, B:E35, B:T36, B:W37, B:Q38, B:E39, B:G40, B:S41, B:L42, B:K43, B:A44, B:S45, B:C46, B:G49, B:Q55, B:D56, B:G57, B:D58, B:L75, B:G79, B:K80, B:D81, B:T108, B:N109, B:Y110, B:E111, B:A112, B:G113, B:K114, B:D115, B:D116, B:V118, B:K119, B:A120, B:P122, B:E129, B:S133, B:Q134, B:N135, B:Q136, B:G137, B:G138, B:K139, B:T140, B:F141, B:V143, B:G144, B:D145, B:Q146, B:I147, B:E162, B:V163, B:L164, B:A165, B:P166, B:G167, B:C168, B:L169, B:D170, B:A171, B:F172, B:P173, B:L174, B:S176, B:A177, B:G180, B:R181, B:S183, B:A184, B:R185, B:P186, B:K187, B:L188, B:K189, B:A190, B:F191, B:L192, B:A193, B:S194, B:P195, B:E196, B:V198, B:N199, B:L200, B:P201, B:I202, B:N203, B:G204, B:N205, B:G206, B:K207, B:Q208	0.744
Chain "A"	A:P1, A:Y2, A:T3, A:P8, A:V9, A:R10, A:A21, A:D22, A:Q23, A:G24, A:Q25, A:S26, A:W27, A:K28, A:E29, A:E30, A:V31, A:V32, A:T33, A:V34, A:E35, A:T36, A:W37, A:Q38, A:E39, A:G40, A:S41, A:L42, A:K43, A:A44, A:S45, A:C46, A:G49, A:Q55, A:D56, A:G57, A:D58, A:L75, A:G79, A:K80, A:D81, A:T108, A:N109, A:Y110, A:E111, A:A112, A:G113, A:K114, A:D115, A:D116, A:V118, A:K119, A:A120, A:P122, A:E129, A:S133, A:Q134, A:N135, A:Q136, A:G137, A:G138, A:K139, A:T140, A:F141, A:V143, A:G144, A:D145, A:Q146, A:I147, A:E162, A:V163, A:L164, A:A165, A:P166, A:G167, A:C168, A:L169, A:D170, A:A171, A:F172, A:P173, A:L174, A:S176, A:A177, A:G180, A:R181, A:S183, A:A184, A:R185, A:P186, A:K187, A:L188, A:K189, A:A190, A:F191, A:L192, A:A193, A:S194, A:P195, A:E196, A:V198, A:N199, A:L200, A:P201, A:I202, A:N203, A:G204, A:N205, A:G206, A:K207, A:Q208	0.743

complete hydrolysis of the chemical can break some or all of the peptide bonds that connect the successive triplets of atoms that make up the chain considered to be the molecule's backbone. This reaction analysis in the IEDB web server (https://www.iedb.org/home_v3.php) a new structure-based tool for the prediction of antibody epitopes and analysis of linear epitope and discontinues epitopes with scores shown in Tables 9 and 10. IEDB web server predicts Chain A and B residues peptides position and location with 5 minimum peptides and 29 number of residues maximum observed in 18 GS protein with the 3-Hydroxyflavone structure shown in Fig. 14 and Studies of the structure and content of peptides and proteins often start with the production of smaller peptides, followed by individual amino acids. An oligopeptide includes only a few amino acids, an octapeptide contains eight, a dipeptide comprises two, an octapeptide is eight, and a polypeptide is numerous. It has been discovered that small peptides act on specific target organs like hormones do [47].

4. Conclusion

Tyrosine shows conventional hydrogen bonding with 3-Hydroxyflavone. From the findings, the Protein Glutathione S-Transferase P (18 GS) was shown to have the best binding affinity with the lowest RMSD and the most stable system state from PES which supports the importance of studying drug metabolism. The IRI, reveals the notable chemical bond interaction and weak interactions. The minimum and maximum of IRI show the efficient embedding scheme for the wave function-based calculations. In addition to providing energy profiles and Lipophilicity, the found tunnels also help the analyses have good absorption. Identification of the tunnel helps to find out the transportation of the protein throughout. Pore-forming proteins (PFPs), which target membranes by creating channels through them, are known as crucial agents in immunity and infection. They achieve this by switching from a form that can be put into a membrane to soluble in an aqueous solution. By way of comparison, because they forecast binding locations utilizing the structures of the same antibody-protein complex's protein antigen and antibody, DOT and PatchDock have an intrinsic advantage over ElliPro. Antibody epitopes in protein antigens with a certain sequence or structure can be predicted using a web-based program called ElliPro. ElliPro has been proposed as a viable research tool for identifying antibody epitopes in protein antigens. The molecular dynamics simulation explains the biomolecular disturbance which is inaccessible through experimental peripheral.

Declaration of competing interest

The authors declare that they have no known competing financial interests or personal relationships that could have appeared to influence the work reported in this paper.

Data availability

Data will be made available on request.

References

[1] Sümeyra Çetinkaya, Kevser Taban Akça, Ipek Süntar, Chapter 3 - flavonoids and anticancer activity: structure-activity relationship, Stud. Nat. Prod. Chem. 74 (2022) 81–115, https://doi.org/10.1016/B978-0-323-91099-6.00017-7.

[2] A. Takahashi, T. Ohnishi, The significance of the study about the biological effects of solar ultraviolet radiation using the exposed facility on the international space station, Biol. Sci. Space 18 (2004) 255–260, https://doi.org/10.2187/bss.18.255.

[3] Sakina BouderiasPéter Teszlák, Gábor Jakab, László Kőrösi, Age- and season-dependent pattern of Flavonol glycosides in Cabernet Sauvignon grapevine leaves, Sci. Rep. 10 (2020), 14241, https://doi.org/10.1038/s41598-020-70706-7.

[4] B.A. Graf, P.E. Milbury, J.B. Blumberg, Flavonol, flavanones, flavanones and human health: epidemiological evidence, J. Med. Food 8 (2005) 281–290, https://doi.org/10.1089/jmf.2005.8.281.

[5] I.C.W. Arts, P.C. H, Hollman Polyphenols and disease risk in epidemiologic studies, Am. J. Clin. Nutr. 81 (2005) 317–325, https://doi.org/10.1093/ajcn/81.1.317S.

[6] A. Panche, S. Chandra, A. Diwan, Alzheimer's and current therapeutics: a review, Asian J. Pharmaceut. Clin. Res. 8 (3) (2015) 14–19.

[7] A. Jager, L. Saaby, Flavonoids and the CNS, Molecules 16 (2011) 1471–1485, https://doi.org/10.3390/molecules16021471.

[8] A.N. Panche, A.D. Diwan, S.R. Chandra, Flavonoids: an overview, J. Nutr. Sci. 5 (e47) (2016), https://doi.org/10.1017/jns.2016.41.

[9] H. Rasouli, S.M. Hosseini-Ghazvini, R. Khodarahmi, Therapeutic potentials of the most studied flavonoids: highlighting antibacterial and antidiabetic functionalities, Stud. Nat. Prod. Chem. (2018) 85–122, https://doi.org/10.1016/b978-0-444-64181-6.00003-6.

[10] E.H. Kelly, R.T. Anthony, J.B. Dennis, Flavonoid antioxidants: chemistry, metabolism and structure-activity relationships, JNB (J. Nutr. Biochem.) 13 (10) (2002) 572–584, https://doi.org/10.1016/S0955-2863(02)00208-5.

[11] Shashank Kumar, Abhay K. Pandey, Chemistry and biological activities of flavonoids: an overview, Sci. World J. 16 (2013), https://doi.org/10.1155/2013/162750.

[12] A.R. Mahmud, T.I. Ema, M.F. Siddiquee, Natural flavonols: actions, mechanisms, and potential therapeutic utility for various diseases, Beni-Suef Univ J Basic Appl Sci 12 (2023) 47, https://doi.org/10.1186/s43088-023-00387-4.

[13] Alan Crozier, Jennifer Burns, Azlina A. Aziz, Amanda J. Stewart, Helena S. Rabiasz, Gareth I. Jenkins, Christine A. Edwards, Michael Ej Lean, Antioxidant flavonols from fruits, vegetables and beverages: measurements and bioavailability, Biol. Res. 33 (2) (2000), https://doi.org/10.4067/S0716-97602000000200007.

[14] O. Benavente-García, J. Castillo, Update on uses and properties of Citrus flavonoids: new findings in anticancer, cardiovascular, and anti-inflammatory activity, J. Agric. Food Chem. 56 (15) (2008) 6185–6205, https://doi.org/10.1021/jf8006568.

[15] S. Nagar, S. Dey, A. Das, S. Basu, 'Flavonoids: recent advances and applications in crop breeding', flavonoid metabolism - recent advances and applications in crop breeding, Intech Open 24 (2023), https://doi.org/10.5772/intechopen.107565.

[16] Guy Raphael Sado Nouemsi, Jean-Bosco Jouda, Peron Bosco Leutcha, Valaire Yemene Matieta, Virginie Flaure Tsague Tankeu, Jenifer Reine Ngnouzouba Kuete, İlhami Çelik, Victor Kuete, Norbert Sewald, Alain Meli Lannang, A new flavonol derivative and other compounds from the leaves of Bauhinia thinning Schum with activity against multidrug-resistant bacteria, Nat. Prod. Res. 37 (16) (2023) 2653–2661, https://doi.org/10.1080/14786419.2022.2128347.

[17] N.P. Bondonno, Y.L. Liu, Y. Zheng, Change in habitual intakes of flavonoid-rich foods and mortality in US males and females, BMC Med. 21 (181) (2023), https://doi.org/10.1186/s12916-023-02873-z.

[18] Susanna Pollastri, Massimiliano Tattini, Flavonols, Old compounds for old roles, Ann. Bot. 108 (7) (2011) 1225–1233, https://doi.org/10.1093/aob/mcr234.

[19] J. Guharay, B. Sengupta, P.K. Sengupta, Protein–flavonol interaction: fluorescence spectroscopic study Proteins, structure function bioinformatics 43 (2) (2001) 75–81, https://doi.org/10.1002/1097-0134(20010501)43:2<75::AID-PROT1019>3.0.CO;2-7.

[20] A Clement Adebamowo, Eunyoung Cho, Laura Sampson, Martijn B. Katan, Donna Spiegelman, Walter C. Willett, Michelle D. Holmes, Dietary flavonols and flavonol-

rich foods intake and the risk of breast cancer, Intl J. cancer 114 (4) (2005) 628–633, https://doi.org/10.1002/ijc.20741.
[21] Gaussian 09, Revision A.02 M.J. Frisch, G.W. Trucks, H.B. Schlegel, G.E. Scuseria, M.A. Robb, J.R. Cheeseman, G. Scalmani, V. Barone, G.A. Petersson, H. Nakatsuji, X. Li, M. Caricato, A. Marenich, J. Bloino, B.G. Janesko, R. Gomperts, B. Mennucci, H.P. Hratchian, J.V. Ortiz, A.F. Izmaylov, J.L. Sonnenberg, D. Williams-Young, F. Ding, F. Lipparini, F. Egidi, J. Goings, B. Peng, A. Petrone, T. Henderson, D. Ranasinghe, V.G. Zakrzewski, J. Gao, N. Rega, G. Zheng, W. Liang, M. Hada, M. Ehara, K. Toyota, R. Fukuda, J. Hasegawa, M. Ishida, T. Nakajima, Y. Honda, O. Kitao, H. Nakai, T. Vreven, K. Throssell, J.A. Montgomery Jr., J.E. Peralta, F. Ogliaro, M. Bearpark, J.J. Heyd, E. Brothers, K.N. Kudin, V.N. Staroverov, T. Keith, R. Kobayashi, J. Normand, K. Raghavachari, A. Rendell, J.C. Burant, S. S. Iyengar, J. Tomasi, M. Cossi, J.M. Millam, M. Klene, C. Adamo, R. Cammi, J. W. Ochterski, R.L. Martin, K. Morokuma, O. Farkas, J.B. Foresman, D.J. Fox, Gaussian, Inc, Wallingford CT, 2016.
[22] C. Lee, W. Yang, R.G. Parr, Development of the Colle-Salvetti correlation-energy formula into a functional of the electron density, Phys. Rev. B Condens. Matter 37 (2) (1998) 785–789, https://doi.org/10.1103/physrevb.37.785.
[23] P. Hohenberg, W. Kohn, Inhomogeneous electron gas, Phys. Rev. 136 (1964) 864–871, https://doi.org/10.1103/PhysRev.136.B864.
[24] AxelD. Becke, Density-functional thermochemistry. III. The role of exact exchange, J. Chem. Phys. 98 (1993) 5648–5652, https://doi.org/10.1063/1.464913.
[25] Michal H. Jamroz, Vibrational Energy Distribution Analysis VEDA 4, Warsaw, 2004, p. 2010, https://doi.org/10.1016/j.saa.2013.05.096.
[26] A.B. Nielsen, A.J. Holder, Gauss View 5.0, User's Reference, GAUSSIAN Inc., Pittsburgh, 2009.
[27] G.M. Morris, R. Huey, W. Lindstrom, M.F. Sanner, R.K. Belew, D.S. Goodsell, A. J. Olson, Autodock4 and AutoDockTools4: automated docking with selective receptor flexibility, J. Comput. Chem. 30 (16) (2009) 2785–2791, https://doi.org/10.1002/jcc.21256.
[28] M. Lundborg, J. Lidmar, B. Hess, The accelerated weight histogram method for alchemical free energy calculations, J. Chem. Phys. 154 (2021), 204103, https://doi.org/10.1063/5.0044352.
[29] H.B. Schlegel, Optimization of equilibrium geometries and transition structures, J. Comput. Chem. 3 (1982) 214–218, https://doi.org/10.1002/jcc.540030212.
[30] J.P. Cornard, L. Vrielynck, J.C. Merlin, J.C. Wallet, Structural and vibrational study of 3-Hydroxyflavone and 3-methoxy flavone, Spectrochim. Acta 51A (5) (1995) 913–923, https://doi.org/10.1016/0584-8539(94)01425-G.
[31] E. Duncan, Mcree, 3 - Computational Techniques, Practical Protein Crystallography, second ed., 1999, pp. 91–269, https://doi.org/10.1016/b978-012486052-0/50005-1. Cp.1.
[32] S. Scheiner, T. Kar, Y. Gu, Strength of the Calpha H... O hydrogen bond of amino acid residues, J. Biol. Chem. 276 (2000) 9832–9837, https://doi.org/10.1074/jbc.M010770200.
[33] Y. Gu, T. Kar, S. Scheiner, Fundamental properties of the CH···O interaction: is it a true hydrogen bond? J. Am. Chem. Soc. 121 (40) (1999) 9411–9422, https://doi.org/10.1021/ja991795g.
[34] Yawen Li, Jacob A. Kreuer, Dustin Wayne Demoin, Silvia S. Jurisson, Carol A. Deakyne, Using potential energy surface scans to examine the bond dissociation energies of trans-ReOS2N2 and [ReOS3N]1− model complexes, Computational and Theoretical Chemistry 1048 (15) (2014), 920140, https://doi.org/10.1016/j.comptc.2014.08.017, 25-34.
[35] T. Lu, F. Chen, Multiwfn: a multifunctional wavefunction analyzer, J. Comput. Chem. 33 (5) (2012) 580–592, https://doi.org/10.1002/jcc.22885.
[36] J.P. Hughes, S. Rees, S.B. Kalindjian, K.L. Philpott, Principles of early drug discovery, Br. J. Pharmacol. 162 (2011) 1239–1249, https://doi.org/10.1111/j.1476-5381.2010.01127.
[37] Q. Gao, L. Yang, Y. Zhu, Pharmacophore based drug design approach as a practical process in drug discovery, Curr. Comput. Aided Drug Des. 6 (1) (2010) 37–49, https://doi.org/10.2174/157340910790980151.
[38] I. Kufareva, R. Abagyan, Methods of protein structure comparison, Homology Modeling (2011) 231–257, https://doi.org/10.1007/978-1-61779-588-6_10, 10.1007/978-1-61779-588-6_10.
[39] A. Castro-Alvarez, A. Costa, J. Vilarrasa, The performance of several docking programs at reproducing protein–macrolide-like crystal structures, Molecules 22 (1) (2017) 136, https://doi.org/10.3390/molecules22010136.
[40] G. Caron, G. Ermondi, R.A. Scherrer, Lipophilicity, Polarity, and Hydrophobicity, Comprehensive Medicinal Chemistry II, 2007, pp. 425–452, https://doi.org/10.1016/b0-08-045044-x/00135-8.
[41] BIOVIA, Dassault Systems, [Discovery Studio Visualizer], [Discovery Studio 2021 Client], Dassault Systems, San Diego, 2021.
[42] Steven M. Ryckbosch1, Paul A. Wender1, S. Vijay, Pande1, Molecular dynamics simulations reveal ligand-controlled positioning of a peripheral protein complex in membranes, Journal of NATURE COMMUNICATIONS (2020), https://doi.org/10.1038/s41467-016-0015-8.
[43] Harvinder Singh, Anupam Raja, Ajay Prakash, Bikash Medhi, Steven M. Ryckbosch1, Paul A. Wender1, S. Vijay, Pande1, Molecular dynamics simulations reveal ligand-controlled positioning of a peripheral protein complex in membranes, Journal of NATURE COMMUNICATIONS (2020), https://doi.org/10.1038/s41467-016-0015-8.
[44] A.A. Yekeen, O.A. Durojaye, M.O. Idris, et al., CHAPERONg: a tool for automated GROMACS-based molecular dynamics simulations and trajectory analyses, Journal of Computational and Structural Biotechnology Journal 21 (2023) 4849–4858.
[45] Z. Prokop, A. Gora, J. Brezovsky, et al., Engineering of protein tunnels: a keyhole-lock-key model for catalysis by the enzymes with buried active sites, in: S. Lutz, U. T. Bornscheuer (Eds.), Protein Engineering Handbook, Wiley-VCH, Weinheim, 2012, pp. 421–464.
[46] Markus Hollander, David Rasp, Moomal Aziz, Volkhard Helms, ProPores2: web service and stand-alone tool for identifying, manipulating, and visualizing pores in protein structures, ACS Journal of Chem. Inf. Model. 61 (4) (2021) 1555–1559, https://doi.org/10.1021/acs.jcim.1c00154.
[47] Ponomarenko Julia, Huynh-Hoa Bui, Wei Li, Nicholas Fusseder, Philip E. Bourne, Alessandro Sette, Bjoern Peters ElliPro, A new structure-based tool for the prediction of antibody epitopes, Journal of BMC Bioinformatics (2020), https://doi.org/10.1186/1471-2105-9-514.